Prediction of jet mixing noise with Lighthill's Acoustic Analogy and geometrical acoustics

Carlos R. S. Ilário[a)]
EMBRAER S.A., Avenue Brigadeiro Faria Lima, 2170, 12227-901, São José dos Campos - SP, Brazil

Mahdi Azarpeyvand
Department of Mechanical Engineering, University of Bristol, Bristol, United Kingdom

Victor Rosa and Rod H. Self
Institute of Sound and Vibration Research, University of Southampton, Southampton, United Kingdom

Júlio R. Meneghini
NDF, Escola Politécnica, University of São Paulo, São Paulo, Brazil

(Received 8 August 2016; revised 11 January 2017; accepted 14 January 2017; published online xx xx xxxx)

A computational aeroacoustics prediction tool based on the application of Lighthill's theory is presented to compute noise from subsonic turbulent jets. The sources of sound are modeled by expressing Lighthill's source term as two-point correlations of the velocity fluctuations and the sound refraction effects are taken into account by a ray tracing methodology. Both the source and refraction models use the flow information collected from a solution of the Reynolds-Averaged Navier-Stokes equations with a standard *k*-epsilon turbulence model. By adopting the ray tracing method to compute the refraction effects a high-frequency approximation is implied, while no assumption about the mean flow is needed, enabling the authors to apply the new method to jet noise problems with inherently three-dimensional propagation effects. Predictions show good agreement with narrowband measurements for the overall sound pressure levels and spectrum shape in polar angles between 60° and 110° for isothermal and hot jets with acoustic Mach number ranging from 0.5 to 1.0. The method presented herein can be applied as a relatively low cost and robust engineering tool for industrial optimization purposes.
[http://dx.doi.org/10.1121/1.4976076]

[JWP] Pages: 1–11

I. INTRODUCTION

Despite great reductions of aircraft noise achieved in the past few decades, the current trend of continuous growth of air traffic worldwide will demand further reduction of noise emission by civil and military aircraft. Due to the inherent complexity of aerodynamic noise generation and propagation phenomena, industrial and academic efforts have been focused on the development of reliable and computationally low-cost noise prediction tools for the aircraft design process. Jet mixing noise is one among the dominant sources of aircraft noise, being more pronounced at take-off condition. As the jet mixing noise has been greatly reduced by increasing the bypass ratio of dual-stream-jet engines, further jet mixing noise reductions are likely to rely on modifications of the nozzle geometry that may result in the use of non-axisymmetric nozzles and therefore very complex three-dimensional flows. For instance, it has been verified both experimentally[1–3] and computationally[4] that the use of chevron nozzles and non-concentric dual-stream nozzles can lead to jet mixing noise reduction.

The development of numerical prediction methods for jet noise is perhaps one of the oldest areas of aeroacoustics. Methods ranging from empirical database[5] to high-fidelity and computationally expensive methods[6–8] have been considered over the past few decades. Nevertheless, a cheap, fast, and reliable numerical method that provides an accurate prediction is still needed to help the optimization process in an industrial context. The hybrid numerical methodology based on a Reynolds Averaged Navier-Stokes (RANS) solution of the flow presented in this paper is seen as an alternative method to fulfill this requirement.

An early application of such hybrid methodology to compute jet mixing noise was presented by Balsa and Gliebe[9] and Balsa *et al.*,[10] who used analytical profiles to describe the mean flow and model the source term of the equation presented by Lilley.[11] The approach was later extended by Khavaran *et al.*[12] and Khavaran and Krejsa[13] to use a numerical RANS $k-\varepsilon$ solution of the mean flow into the so-called MGBK (Mani, Gliebe, Balsa, and Khavaran) method; thus consolidating the use of a RANS $k-\varepsilon$ and an acoustic analogy to model jet mixing noise.

The idea was further explored by Tam and Auriault,[14] who modeled the sound sources via an analogy with the kinetic theory of gases. They added the proposed source term to an adjoint formulation of the Linearized Euler Equations, therefore departing from the use of an acoustic analogy; their predictions of far-field sound pressure level (SPL) showed good agreement with measurements. Morris and Farassat[15] showed that although not explicitly an

a)Electronic mail: carlos.ilario@embraer.com.br

acoustic analogy, Tam and Auriault's method is akin to what can be derived from an acoustic analogy, and showed that the improvements by Tam and Auriault's method was the better description of the turbulence statistics relevant for the description of the sources of sound.

Self[16] followed by proposing a model based on Lighthill's Acoustic Analogy (LAA) with an improved description of the relevant turbulence statistics based on empirical evidence by Harper-Bourne.[17] The main improvement was the consideration of frequency-dependent time and length-scales when modeling velocity correlations present in LAA's source term. The proposed model resulted in good agreement with experimental data, notably with a better description of the decay at low and high frequencies when compared to the LAA-based method of Morris and Farassat.[15] Self and Azarpeyvand[18,19] and Azarpeyvand and Self[20] further developed the idea of frequency-dependent scales of velocity correlations by proposing a new time scale which was applied to the MGBK method.

In this paper a source model based on the LAA with the new time scale of Refs. 18–20 is presented. The resulting statistical source is shown to result in a good description the far-field spectrum at 90°. To overcome the shortcoming of LAA that ignores effects of propagation, a geometrical acoustics approximation is applied. The application of geometrical acoustics is not new in jets,[21–23] but it is, to the authors best knowledge, for the first time coupled to a source model based on the LAA to predict jet mixing noise instead of just analyze aspects of it. Another way to compute the propagation effects is to solve the adjoint formulation of the linearized Euler equations using a finite difference method (FDM).[24] Using a FDM, however, increases the computational cost of the overall prediction method as the FDM is expensive and known to generally require a mesh of higher quality (finer and structured) than the RANS mesh. The ray tracing method used in this paper, in contrast, needs only to interpolate the results from the RANS into a coarser mesh. The main objective of this paper is therefore to introduce and benchmark a novel hybrid aeroacoustics method that can be applied to predict the far-field noise from arbitrary three-dimensional jets. The method was created with the goal of providing the ability for both the analysis and the optimization of nozzles that would be compatible with novel configurations, yet requiring relatively low computational cost.

The remainder of the paper is organized as follows. Section II deals with the source and propagation models developed as part of this work. The experimental setup and solution of the mean flow are presented in Sec. III. Also in Sec. III the far-field noise predictions for jets at different Mach numbers and temperature ratios predicted using the new model will be compared against the available experimental data at different angles. Results will be presented for jet noise prediction at 90°, source distribution, flow factor, and jet noise directivity. Finally, Sec, IV concludes the paper.

II. MATHEMATICAL MODEL

The mathematical modeling of the new jet noise prediction tool is provided in this section. The far-field noise can be predicted by coupling the source and propagation models, presented in Secs. II A and II B. The models are derived separately, emphasizing the fact that they are completely independent and can be used in isolation.

A. Source model

The starting point of the source model is the Lighthill equation,[25] as presented by Ribner.[26] The far field spectrum can be written as

$$P(\boldsymbol{x};\omega) = \frac{1}{(4\pi r)^2}\frac{1}{a_0^4}\bar{\rho}^2 D_f^{-5} d_{ijkl}\int \Phi \mathcal{F}[I_{ijkl}]\,\mathrm{d}^3\boldsymbol{y}, \tag{1}$$

where $r = |\boldsymbol{x}|$ is the distance to the far-field observer, and $\boldsymbol{x}$ and $\boldsymbol{y}$ are, respectively, the observer and source locations. The coordinate system (r, θ, φ) is shown in Fig. 1. In Eq. (1), a_0 is the reference speed of sound, $\bar{\rho}$ is the mean fluid density, D_f is the Doppler factor $(1 - M_c\cos\theta)$, d_{ijkl} is the tensor giving the quadrupolar directivity, Φ is the flow factor (introduced in the next section), $\mathcal{F}$ denotes the Fourier transform, and I_{ijkl} represents the contribution from fourth-order velocity correlations.

The convective Mach number (M_c) is assumed to depend on the local Mach number (U_1/a) and the nozzle exit Mach number $(M = U/a_0)$ and is given by[12]

$$M_c = \frac{1}{4}\left(\frac{U_1}{a}\right) + \frac{1}{3}M, \tag{2}$$

where U_1 is the local mean axial velocity, U the jet-exit velocity, and a the local mean sound speed.

The tensor I_{ijkl} represents the contribution of the fourth-order velocity correlation terms and is given by

$$I_{ijkl}(\tau) = \int \frac{\partial^4}{\partial \tau^4}\overline{v_i v_j v_k' v_l'}\,\mathrm{d}^3\boldsymbol{\xi}, \tag{3}$$

where $v_i = U_i + u_i$ is the instantaneous velocity vector, the prime indicates that the property is evaluated at a different

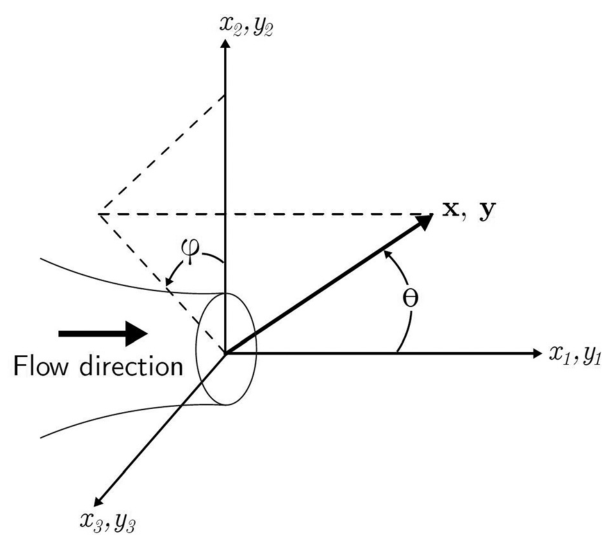

FIG. 1. Cartesian and spherical coordinate systems.

instant in time (separated by τ) and different location in space (separated by $\boldsymbol{\xi} \equiv \{\xi_1, \xi_2, \xi_3\}$).

Only the fluctuating velocities are considered as efficient sources of mixing noise, so that Eq. (3) can be written as

$$I_{ijlk}(\tau) = \int \frac{\partial^4}{\partial \tau^4} \overline{u_i u_j u'_k u'_l} \mathrm{d}^3 \boldsymbol{\xi}, \qquad (4)$$

which is equivalent to the "self-noise" component as by Ribner.[26]

To model the cross-correlation in Eq. (4) some assumption about turbulence is necessary. We consider that turbulence is isotropic and locally homogeneous, so it follows a normal joint probability between u_i and u'_j. Therefore $\overline{u_i u_j u'_k u'_l}$ can be expressed in terms of second-order correlations as[26,27]

$$\overline{u_i u_j u'_k u'_l} = \overline{u_i u_j}\ \overline{u'_k u'_l} + \overline{u_i u'_k}\ \overline{u_j u'_l} + \overline{u_i u'_l}\ \overline{u_j u'_k}. \qquad (5)$$

These second-order correlations can, in turn, be expressed in terms of independent spatial and temporal correlation functions as[26]

$$\overline{u_i u'_j}(\boldsymbol{\xi}, \tau) = R_{ij}(\boldsymbol{\xi}) g(\tau). \qquad (6)$$

Noting that $\partial^4 \left(\overline{u_i u_j}\ \overline{u'_k u'_l} \right) / \partial \tau^4 = 0$ as $\overline{u_i u_j}$ and $\overline{u'_k u'_l}$ are independent of time separation (τ), and using Eqs. (5) and (6), Eq. (4) can be rewritten as

$$I_{ijkl} = \frac{\partial^4 g^2}{\partial \tau^4} \int (R_{ik} R_{jl} + R_{il} R_{jk}) \mathrm{d}^3 \boldsymbol{\xi}. \qquad (7)$$

Again invoking the assumption of isotropic and locally homogeneous turbulence, the spatial correlation term, R_{ij}, takes the form[27]

$$R_{ij} = \overline{u_1^2} \left[\left(f + \frac{1}{2} |\xi| f' \right) \delta_{ij} - \frac{1}{2} f' \frac{\xi_i \xi_j}{|\xi|} \right], \qquad (8)$$

where f is a function of the separation vector ξ, and $f' = df/d\xi$. Among different possibilities,[26] f is assumed here to take a Gaussian distribution form

$$f(\xi) = \exp\left(-\pi \frac{\xi^2}{L^2} \right), \qquad (9)$$

where L is the length-scale at the source location.

With the substitution of Eqs. (8) and (9) in Eq. (7) and performing the integral over the source region (ξ), the term I_{ijkl} reduces to

$$I(\tau) = \frac{\rho^2}{2\sqrt{2}} k^2 L^3 \frac{\partial^4 g^2(\tau)}{\partial \tau^4}, \qquad (10)$$

where k is the local mean turbulent kinetic energy.

Here the directivity index $ijkl$ is dropped to emphasize that the source is isotropic due to the assumption of isotropic turbulence. Thus the far-field directivity is modeled by the convective amplification given by D_f^{-5} and refraction (presented in Sec. II B).

It is assumed that the temporal correlation function, g, also takes a Gaussian distribution form, as

$$g(\tau) = \exp\left(-\tau^2/\tau_0^2 \right), \qquad (11)$$

where τ_0 is the time scale at the source location. Taking the Fourier transform of $\partial^4 g^2 / \partial \tau^4$ in Eq. (10) leads to

$$I(\Omega) = \frac{\sqrt{\pi}}{4} k^2 L^3 \tau_0 \Omega^4 \frac{\sqrt{2\pi}}{2} \exp\left(-\frac{\tau_0^2 \Omega^2}{8} \right), \qquad (12)$$

where Ω is the modified frequency

$$\Omega = \omega \sqrt{(1 - M_c \cos\theta)^2 + \left(\alpha k^{1/2}/a_0 \right)^2}, \qquad (13)$$

where α is an experimental parameter with value of 0.5.[12]

The length-scale L can be calculated using parameters obtained from a RANS $k - \varepsilon$ simulation as[12,28]

$$L = c_\ell \frac{k^{3/2}}{\varepsilon}, \qquad (14)$$

where c_ℓ is an empirical constant and ε is the turbulent dissipation rate. The time scale τ_0 takes the form

$$\tau_0 = c_\tau \frac{k}{\varepsilon}, \qquad (15)$$

where c_τ is an empirical constant.

Rewriting the length-scale in terms of the time scale Eq. (12) takes the form

$$I(\Omega) = \frac{\sqrt{\pi}}{4} \frac{c_\ell^3}{c_\tau^3} k^{7/2} \rho^2 \tau_0^4 \Omega^4 \exp\left(-\frac{\tau_0^2 \Omega^2}{8} \right), \qquad (16)$$

which gives the spectrum of the source emitting from a single correlated volume of turbulence in the jet. Note that the coefficient c_τ is in the definition of the time scale τ_0; so even if the term c_ℓ^3/c_τ^3 were combined as a single coefficient, c_τ would still be needed for τ_0.

In Refs. 18–20 a new time scale was proposed, which is shown to better describe the energy transfer process related to the jet noise generation process. The new time scale is given by

$$\tau_0^\star = \tau_0 \left(\frac{L}{D} \right)^{2/3}, \qquad (17)$$

where D is the nozzle diameter. Replacing τ_0 with $\tau_0^\star$ in Eq. (16) and inserting the result in Eq. (1) yields

$$P(\boldsymbol{x}; \omega) = \frac{1}{64\pi^{3/2}} \frac{1}{r^2 a_0^4} \frac{c_\ell^3}{c_\tau^3} \int \Phi(\boldsymbol{x}|\boldsymbol{y}) D_f^{-5} \bar{\rho}^2 k^{7/2} \times \tau_0^{\star 4} \Omega^4 \exp\left(-\frac{\Omega^2 \tau_0^{\star 2}}{8} \right) \mathrm{d}^3 \boldsymbol{y}. \qquad (18)$$

In Sec. II B the ray tracing solution of the sound propagation through the jet flow is presented and the associated flow factor, Φ, is introduced.

B. Propagation model

A major drawback of LAA is that the refraction of sound by the mean flow is difficult to be accounted for because of the assumptions needed to describe the source term. Therefore alternative methods, for instance, through the definitions of the "Flow Factor" using the asymptotic solution of Lilley's equation, are necessary to model the effect of the mean flow. In this paper, we tackle this problem by introducing a Flow Factor parameter to take into account the sound-flow refraction phenomenon using a high-frequency approximation of sound propagation in non-uniform media by geometrical acoustics. The derivation of the ray tracing equations presented in this section follows the description of Pierce.[30] The obvious advantage of the proposed technique to Lilley's asymptotic solution is its versatility and the possibility of using the new method for complex and asymmetric jet flows.

If x_p^{ray} is a point on the wavefront defining the position of a ray, this point will follow the wavefront with velocity

$$\frac{d\boldsymbol{x}_p^{\text{ray}}}{dt} = \boldsymbol{v}\left(\boldsymbol{x}_p^{\text{ray}}, t\right) + \boldsymbol{n}\left(\boldsymbol{x}_p^{\text{ray}}, t\right) a\left(\boldsymbol{x}_p^{\text{ray}}, t\right), \tag{19}$$

where $\boldsymbol{n}$ is the vector normal to the wavefront. It is possible to calculate the ray path by integrating Eq. (19) with respect to time if $\boldsymbol{v}$, a, and $\boldsymbol{n}$ are known. However, the evaluation of $\boldsymbol{n}$ requires the reconstruction of the wavefront at each space time interval, which is not straightforward as it requires the position of all neighboring rays. A simpler solution is possible by using the wave-slowness vector, which is also normal to the wavefront and is defined as

$$\boldsymbol{s} = \frac{\boldsymbol{n}}{a + \boldsymbol{v} \cdot \boldsymbol{n}}, \tag{20}$$

which can be written in the following form after some mathematical manipulation:

$$s^2 = \frac{\Omega^2}{a^2}, \tag{21}$$

where $\Omega = 1 - \boldsymbol{v} \cdot \boldsymbol{s}$. Equation (21) accounts for the slowness factor variation in space with the mean velocity and sound speed field.

The ray-tracing equations can be written in the Cartesian coordinate system,[30] which are represented by six ordinary differential equations that couple the ray position and the slowness vector

$$\frac{dx_i^{\text{ray}}}{dt} = U_i + \frac{a s_i}{1 - U_j s_j}, \tag{22}$$

$$\frac{ds_i}{dt} = -\frac{1 - U_j s_j}{a}\frac{\partial a}{\partial x_i} - s_j \frac{U_j}{x_i}. \tag{23}$$

The above system is solved by integrating Eqs. (22) and (23) in time using a fourth-order Runge–Kutta method, while the mean flow properties, i.e., U_i and a and associated derivatives, are obtained by interpolation from a numerical RANS flow-field solution. The equations are integrated until the ray exits the RANS simulation domain (i.e., unidirectional flow), from where it is considered to follow a straight line to the far-field observer position.

The ray tracing equations give no direct information about the acoustic pressure amplitude. It is therefore necessary to resort to the concept of ray-tubes and conservation of energy which leads to the Blokhintzev invariant.[30,31] The invariant shows that along a given ray

$$\frac{\overline{p^2} V A}{(1 - U_i s_i)\rho a^2} = \text{const}, \tag{24}$$

where p is the acoustic pressure, $V = |d\boldsymbol{x}^{\text{ray}}/dt|$ is the magnitude of the ray velocity vector, and A is the ray-tube area. Using Eq. (24) for a ray traced from the source location, $\boldsymbol{y}$, to the far-field observer, $\boldsymbol{x}$, results in

$$\frac{\overline{p^2}|_{\boldsymbol{x}}}{\overline{p^2}|_{\boldsymbol{y}}} = \frac{\left.\dfrac{V}{(1 - U_i s_i)\rho a^2}\right|_{\boldsymbol{y}} A|_{\boldsymbol{y}}}{\left.\dfrac{V}{(1 - U_i s_i)\rho a^2}\right|_{\boldsymbol{x}} A|_{\boldsymbol{x}}}, \tag{25}$$

which quantifies the change in the pressure amplitude along a given ray from the source location to the far-field observer. However, this is not the amplitude change needed to compute the flow factor Φ. The aim is to calculate the difference of pressure amplitude in the far-field between a ray traced over a quiescent medium and traced over the jet mean flow, both launched from the same source location. Hence, the flow factor used in our methodology is defined as

$$\Phi(\boldsymbol{x}, \boldsymbol{y}) = \frac{\overline{p^2}|_{\boldsymbol{x},\text{flow}}}{\overline{p^2}|_{\boldsymbol{x},\text{quiescent}}}, \tag{26}$$

where $\overline{p^2}|_{\boldsymbol{x},\text{flow}}$ is evaluated at the observer location for a ray launched from $\boldsymbol{y}$ and traced over the mean flow and $\overline{p^2}|_{\boldsymbol{x},\text{quiescent}}$ is evaluated at the observer location with the ray traced over a quiescent medium (i.e., a straight line between source and observer).

To compute Φ from Eq. (25) it is assumed that

$$\overline{p^2}|_{\boldsymbol{y},\text{flow}} = \overline{p^2}|_{\boldsymbol{y},\text{quiescent}}, \tag{27}$$

$$\left.\frac{V}{(1 - U_i s_i)\rho a^2}\right|_{\boldsymbol{x},\text{quiescent}} = \left.\frac{V}{(1 - U_i s_i)\rho a^2}\right|_{\boldsymbol{y},\text{quiescent}} \tag{28}$$

and

$$A|_{\boldsymbol{y},\text{flow}} = A|_{\boldsymbol{y},\text{quiescent}}. \tag{29}$$

The flow factor can therefore be given by

$$\Phi(\boldsymbol{x}, \boldsymbol{y}) = \frac{\left.\dfrac{V}{(1 - U_i s_i)\rho a^2}\right|_{\boldsymbol{y},\text{flow}} A|_{\boldsymbol{x},\text{quiescent}}}{\left.\dfrac{V}{(1 - U_i s_i)\rho a^2}\right|_{\boldsymbol{x},\text{flow}} A|_{\boldsymbol{x},\text{flow}}}. \tag{30}$$

The first fraction on the right-hand side of Eq. (30) is evaluated using the ray tracing solution and the flow information obtained from the RANS solution. The ray-tube area

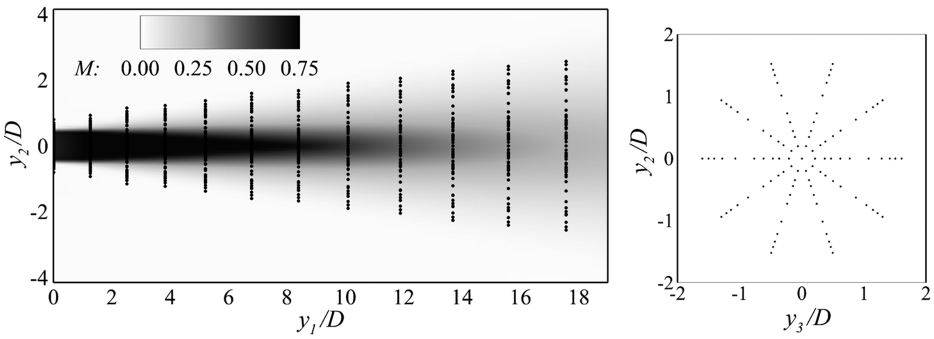

FIG. 2. Black dots show source locations for ray tracing method.

ratio cannot be computed directly from the ray tracing solution and is approximated by the ray density ratio in the far field.

To compute the ray density ratio, the far-field is represented as a spherical shell, discretized in spatial elements ($\sim 10^4$ far-field bins for the results in this paper), and a large number of rays ($\sim 6 \times 10^5$) are launched from each source location within the jet flow. To achieve a uniform spatial distribution, the far-field bins and the ray launching angles are defined using the vertices of a geodesic sphere.[32–34] Each ray is assigned to a far-field bin by comparing its far-field location with the far-field bin coordinates. The number of rays assigned to each far-field bin is summed as N_{flow} for rays traced through the mean flow and $N_{\text{quiescent}}$ when a quiescent medium is considered. Thus, Eq. (31) can be written as

$$\Phi(\boldsymbol{x}, \boldsymbol{y}) = \frac{\left.\dfrac{V}{(1 - U_i s_i)\rho a^2}\right|_{\boldsymbol{y},\text{flow}}}{\left.\dfrac{V}{(1 - U_i s_i)\rho a^2}\right|_{\boldsymbol{x},\text{flow}}} \frac{N|_{\boldsymbol{x},\text{flow}}}{N|_{\boldsymbol{x},\text{quiescent}}}. \tag{31}$$

The flow factor (Φ) must now be calculated for a finite number of source locations $\boldsymbol{y}$ ($\sim 10^3$) within the jet domain. The locations are non-uniformly distributed in the jet domain, with clusters of sources in regions of high velocity gradients and turbulent kinetic energy. An example of the distribution of about 1700 sources for a single-flow jet is presented in Fig. 2. Having presented the source and propagation models, in Sec. III results for single-stream jets at different operating conditions will be presented and discussed.

III. RESULTS AND COMPARISONS

The canonical circular single-stream jet has been extensively studied analytically, numerically, and experimentally.[15,26,29] In this section, some aspects of the sound generation of a circular single-stream jet at different operating conditions are presented and discussed using the method developed in Sec. II. A total number of 12 operating conditions have been considered. They comprise three Mach numbers: $M = 0.5$, 0.75, and 1.0 (reference sound speed in the far-field is 340 m/s); and four temperature ratios: TR = 1.0, 1.5, 2.0 and 2.5 (where TR is the ratio between the jet-exit temperature and the reference temperature of 288 K in the surrounding medium). The nozzle in this study is shown in Fig. 3. AQ6

For each of the 12 cases, measurements of far-field spectra are available and a corresponding CFD (Computational Fluid Dynamics) RANS $k - \varepsilon$ solution is conducted. The measurements of far-field noise were carried out in the Noise Test Facility at QinetiQ Pyestock, United Kingdom. The facility comprises of a chamber of area $27 \times 26\ \text{m}^2$ and 14 m height, being anechoic down to approximately 90 Hz. Results used in this paper are recorded using a microphone array at 12 m ($\approx$120 D) from the nozzle exit and are presented as 1 m loss-less data.

A brief description of the mean flow solution is presented in Sec. III A, followed by a presentation of the results computed with the source and propagation models presented in this paper. The main emphasis of the results is to show the accuracy in the far-field noise prediction and the possibility to account for three-dimensional propagation effects for a realistic spreading jet.

A. Mean flow solution

The mean flow is computed with a standard finite volume second-order commercial CFD solver.[35] The continuity, momentum, and energy equations are solved for a compressible gas, along with the equation of state for an ideal gas. To model the jet flow the standard $k - \varepsilon$ model is used, with the two additional equations solved using the standard coefficients.

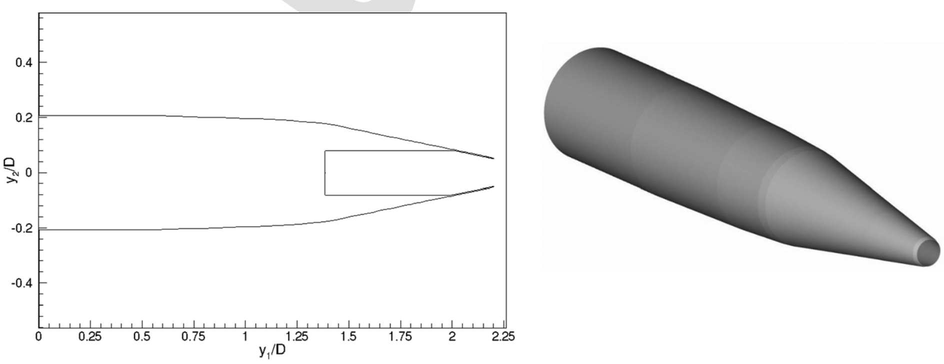

FIG. 3. Geometry of the $D = 0.1016$ m nozzle.

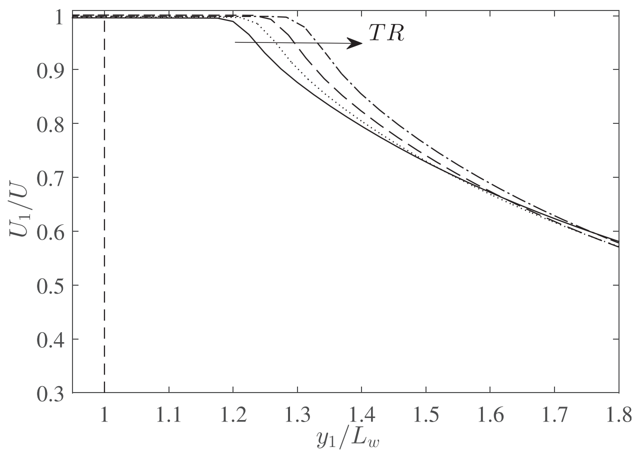

FIG. 4. Centerline axial velocity decay with axial distance normalized by empirical length of potential core (L_w) (Ref. 37) for $M = 0.75$ jets. Solid line, TR = 1; dotted line, TR = 1.5; dashed line TR = 2; and dashed-dotted line TR = 2.5. The parameter L_w was computed for each temperature ratio. The fact that the curves start to decay at higher y_1/L_w shows that the over-prediction of the potential core length by RANS $k-\varepsilon$ worsens with increased temperature ratio.

Figure 4 shows the normalized velocity along the jet center-line for a $M = 0.75$ jet at different temperature ratios, TR = 1, 1.5, 2, and 2.5. Results are presented in terms of the empirical potential core length as defined by Witze[37]

$$L_w = (D/2)\left[0.08(1-0.16M)\mathrm{TR}^{0.28}\right]^{-1}, \quad (32)$$

so that $y_1/L_w = 1$ represents the end of potential core for a given M and TR. As known, the predictions with the standard $k-\varepsilon$ model result in an over-prediction of the potential core length. Although several turbulence model corrections have been proposed and discussed in the literature,[36] we have used the standard model as it is widely available and used in an industrial context. As can be seen, the over-prediction grows with the temperature ratio (TR), making the predictions less reliable for very hot jets. Despite the obvious shortcomings of the $k-\varepsilon$ model, the mean flow solution is still capable of providing good jet noise prediction, which will be discussed in Secs. III B–III E.

B. Far-field noise prediction at 90°

RANS-based prediction methods[14–16,38,39] generally require empirically calibrated coefficients to relate the statistical properties of the mean flow from RANS $k-\varepsilon$ to the relevant properties of the sound generation process (or, more recently, calibrated with transient numerical solutions).[40,41] Contrary to other methods that rely on three coefficients (amplitude, length-scale, and time scale), the method presented in this paper only needs two coefficients, c_ℓ and c_τ. The values for these coefficients are computed by comparing the predicted SPL with the measured noise data at $\theta = 90°$. The optimum values vary slightly with Mach number but more significantly with temperature ratio. The jet noise predictions for isothermal jets are performed using $c_\tau = 0.43$ and $c_\ell = 0.8$. For hot jets c_τ is kept at the same value while c_ℓ is allowed to vary from 0.8 for TR = 1 to around 1.9 for TR = 2.5.

Figure 5 shows a comparison of the predicted SPL at $\theta = 90°$ with measured far-field data for the 12 cases considered, in the absence of refraction effects. The good agreement observed, both in terms of the overall shape of the spectra and the peak frequency location at different Mach numbers, confirms that the source model captures well the physics of the noise generation mechanism. The need of calibration for different temperature ratios is a result of neglecting the additional source terms related to hot jets, such as the density variation. Nevertheless, by showing that c_τ can be kept constant while only c_ℓ needs further calibration to properly capture the SPL spectra of the hot jets is an indication that this additional source has a similar nature of the source already modeled.

C. Source location results

The source model developed in Sec. II can be used to study the distribution of the sound sources in the jet plume. To do so, the volume integral in Eq. (18) is computed only in the $y_2 - y_3$ plane so the contribution to the far-field noise from a slice of the jet is computed as $P_{\mathrm{slice}}(\boldsymbol{x}, \omega, y_1)$.

Figure 6 shows the results for an observer located at 90° in the far-field. Different Strouhal numbers ($\mathrm{St} = fD/U$) for isothermal jets at Mach numbers of 0.5, 0.75, and 1 are considered. The source amplitude results are normalized by its value at St = 0.2. As expected, results have shown the higher-frequency sources are located near the nozzle exit and the most energetic sources are slightly after the end potential core (if the overprediction of the potential core length shown in Fig. 4 is considered, the peak in Fig. 6 moves closer to the end of potential core). The collapsing of the results for the three different Mach numbers is evidence that the source distribution is self-similar in frequency and space, with the driving parameters being the Strouhal number for frequency and y_1/L_w for space.

D. Sound-flow interaction effects

The effect of refraction can further be analyzed in isolation by plotting the flow factor computed using the ray tracing and ray density ratio. The flow factor $\Phi(\boldsymbol{x}|\boldsymbol{y})$ gives the amplification or reduction of the SPL due to the refraction for the noise collected at a microphone location ($\boldsymbol{x}$) due to a noise source at ($\boldsymbol{y}$) within the jet plume. In this section, the flow factor results in dB, i.e., $(10\log\Phi)$, are presented in two forms: (i) by fixing the source location ($\boldsymbol{y}$) and varying the observer location ($\boldsymbol{x}$) in the far-field over $0° < \theta < 180°$ and $0° < \phi < 360°$, and (ii) fixing the observer location ($\boldsymbol{x}$) and varying the source location (y_1 and y_2) within the jet plume. This enables a better understanding of the three-dimensional nature of the refraction effects appearing even in the axisymmetry nozzle studied in this paper.

First, the effect of refraction is analyzed for sound emitted from sources on the lip-line of a $M = 0.75$ jet with TR = 1, see Fig. 7. The sources are positioned along the nozzle lip-line ($y_2/D = 0.5$), i.e., within the jet shear-layer where the turbulent kinetic energy (k) peaks and, according to $P(\omega) \propto k^{7/2}$ relation, from Eq. (18), can be considered as one of the most important noise generation regions. Figure 7

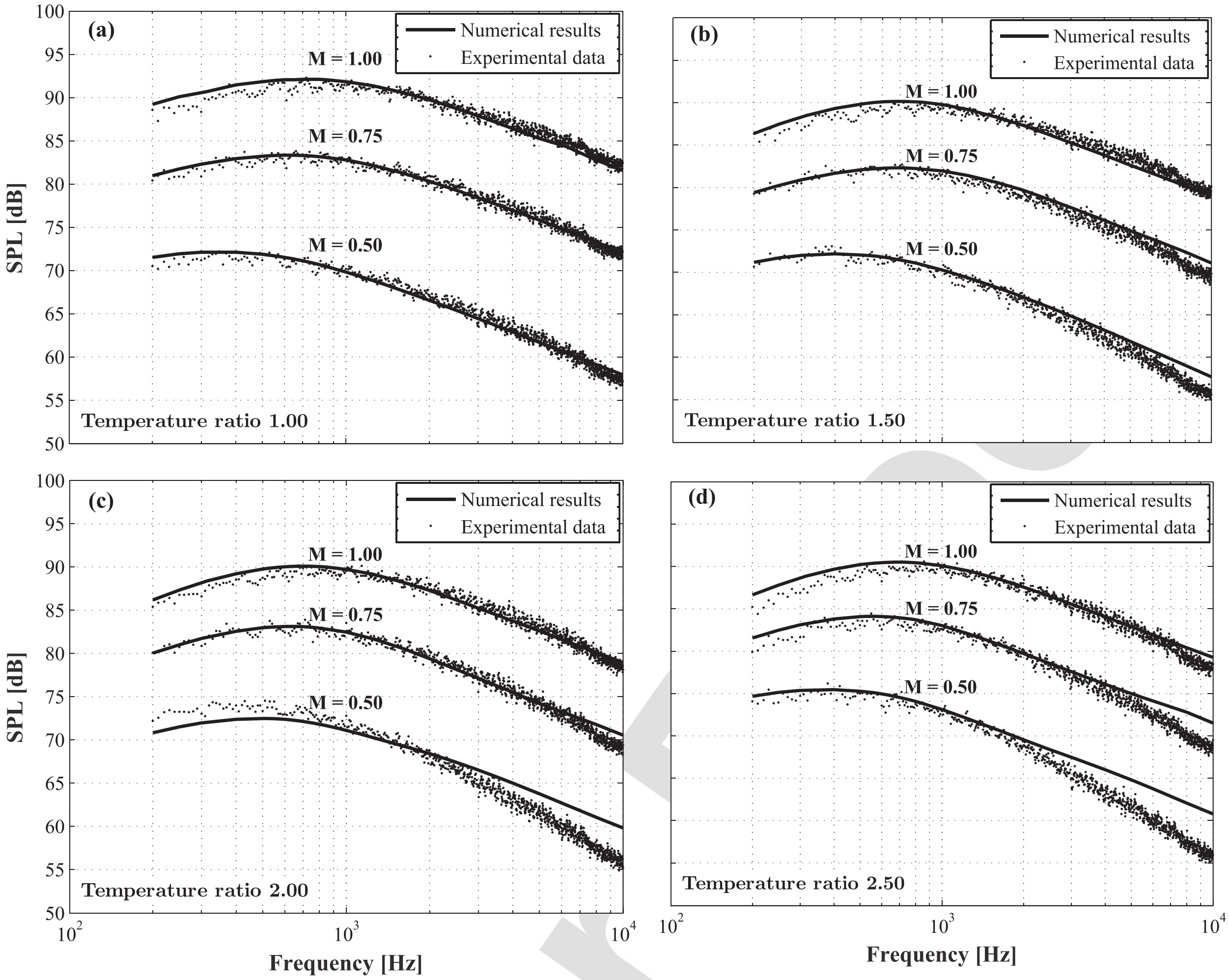

FIG. 5. Far-field SPL predictions and measurements at 90° for different M and TR: (a) TR = 1.00, (b) TR = 1.50, (c) TR = 2.00, (d) TR = 2.50.

shows the contour plots of the flow factor, where the negative Flow Factor indicates reduction of SPL due to the flow refraction and positive values show sound amplification. The white area in the plots represents the shadow zone where no rays are collected and the ray tracing approximation is no longer valid. The effects of refraction are presented as a function of the polar and azimuthal angles of the observer for sound emitted from four different source locations on the lip line with different downstream locations ($y_1/D = 1$, 2.6, 5, and 10).

For a source located at $y_1/D = 1$ and $y_2/D = 0.5$, the shadow zone has a variable shape along the azimuthal coordinate, see Fig. 7(a). The dashed line A shows that the critical angle defining the shadow zone occurs at about 60° and it goes from $\varphi \approx 10°$ to 160°. With increasing φ, a new shadow zone area will appear, shown as region B. The change of the critical angle down to $\theta = 20°$ for observers in the opposite side of the source is an interesting phenomenon which has not previously been shown. An area of high intensity, i.e., sound amplification, can also be observed within region B, at about $\theta = 65°$, which is due to the rays entering the potential core of the jet, i.e., the rays that are not being totally reflected. The potential core in this situation acts like a lens for these rays, focusing them over a small region. This shows the importance of the effect of the potential core on sound propagation within the jet plume and the far-field noise amplification, particularly for asymmetric jets. Another area of strong sound amplification for observers below the jet occurs at $\varphi \approx 90°$ and $\theta \approx 110°$, shown as Region C.

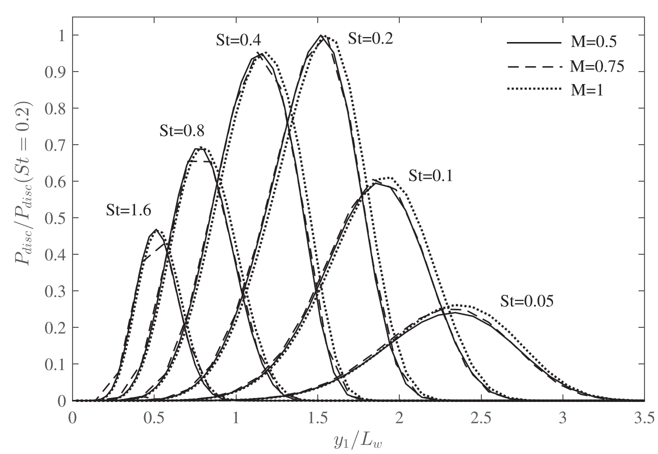

FIG. 6. Source distribution for isothermal jets as a function of axial distance for different Strouhal number (St = fD/U), normalized by the maximum of the distribution for St = 0.2. Axial coordinate normalized by potential core length (L_w). Solid lines, $M = 0.5$; dashed lines, $M = 0.75$; dotted lines, $M = 1$.

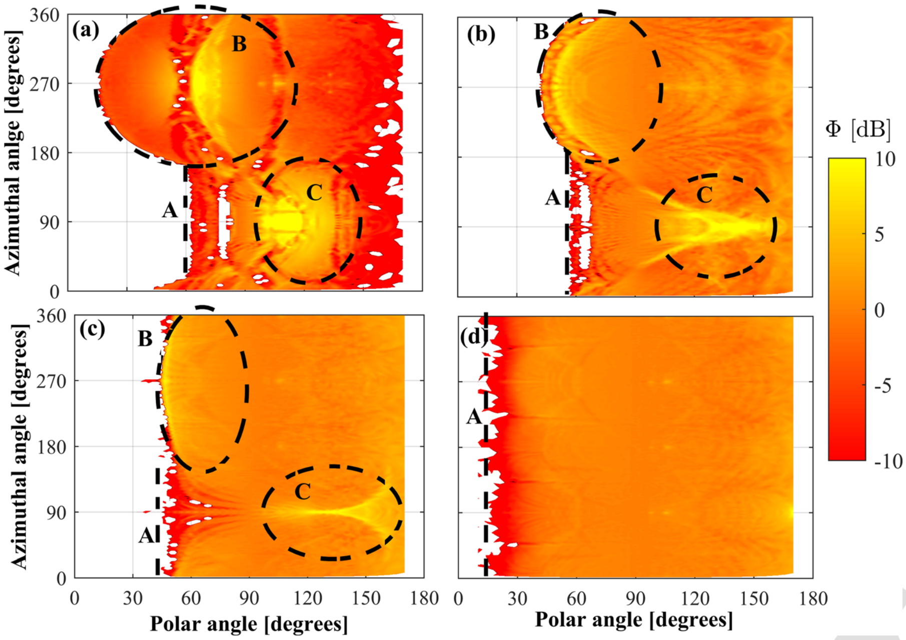

FIG. 7. (Color online) Flow factor for sources on the lip line of isothermal jet with $M = 0.75$. All sources are in the azimuthal angle of $\varphi = 90°$, with varying downstream location: (a) $y_1/D = 1$, (b) $y_1/D = 2.6$, (c) $y_1/D = 5$, and (d) $y_1/D = 10$.

Moving further downstream, for a point source located at $y_1/D = 2.6$ and $y_2/D = 0.5$, Fig. 7(b), the Flow Factor results change considerably, altering not only its shape but also the critical angle to $\approx 40°$. Also, the noise amplification region before the shadow zone still plays an important role for this source location. Regarding region C, the peak area is becoming sharper and it is spreading along the polar angles. This can be understood by the fact that more rays are being convected by the flow due to the jet spreading. A similar trend has been observed for a source located near the end of the potential core at $y_1/D = 5$ and $y_2/D = 0.5$, see Fig. 9(c). The main differences are that the critical angle (shown by line A) goes down to $\approx 45°$ and varies less with φ. Since the point source is now located near the end of the potential core, the acoustic lens effect of the potential core, as observed in Fig. 7(a) (region B), become less obvious and Region B shrink to a very small θ area over $180° < \phi < 360°$. Region C also moves to higher polar angles of about $\theta = 140°$. The results in Fig. 7(d) show that in the case of a source positioned at $y_1/D = 10$ and $y_2/D = 0.5$, in the absence of strong velocity gradient, the blockage effect (for $\varphi \approx 270°$) is minimized and it is no longer possible to identify regions B and C. Following the trend from the previous source locations, the critical angle shown by line A is further reduced to $\theta \approx 20°$ and becomes effectively axisymmetric.

The results in Figs. 8 and 9 show the flow factor for different regions of the jet for an observer at $\varphi = 90°$ (i.e., above the plane of the figure) and two different polar angles ($\theta = 50°$ and $\theta = 90°$). Results are presented for an isothermal and TR $= 2.5$ jet. As expected, the refraction factor in the case of an observer at $\theta = 90°$ is almost zero, indicating

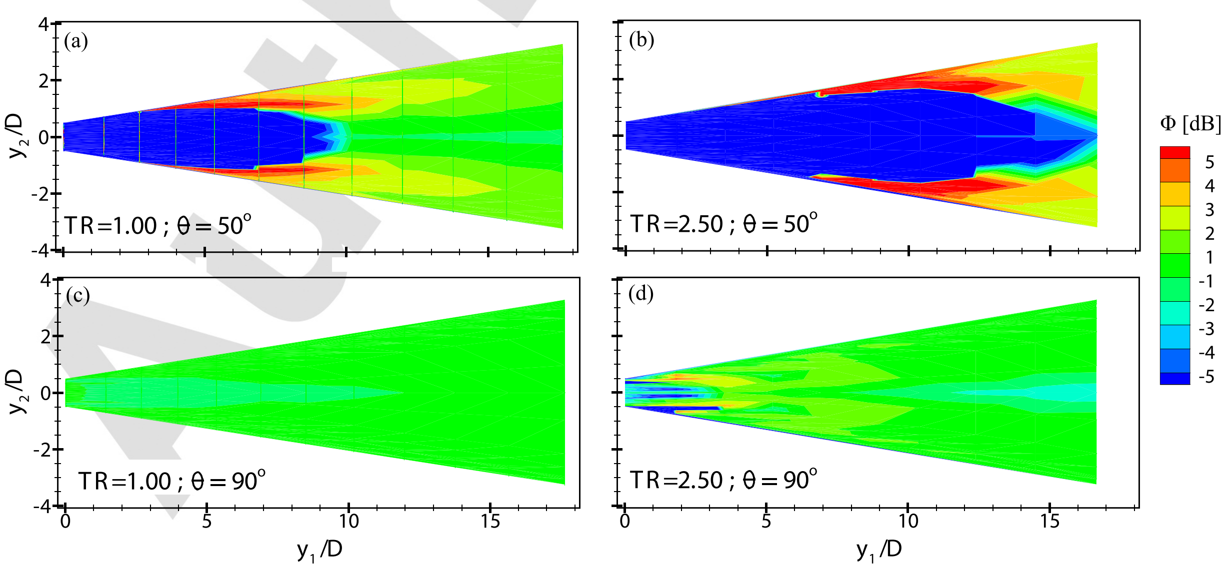

FIG. 8. (Color online) Flow factor for jet with $M = 0.75$ and different temperature ratios: (a) and (c), TR $= 1$; (b) and (d), TR $= 2.5$. Observer above plane of figure ($\varphi = 90°$) and different polar angles: (a) and (b), $\theta = 50°$; (c) and (d), $\theta = 90°$.

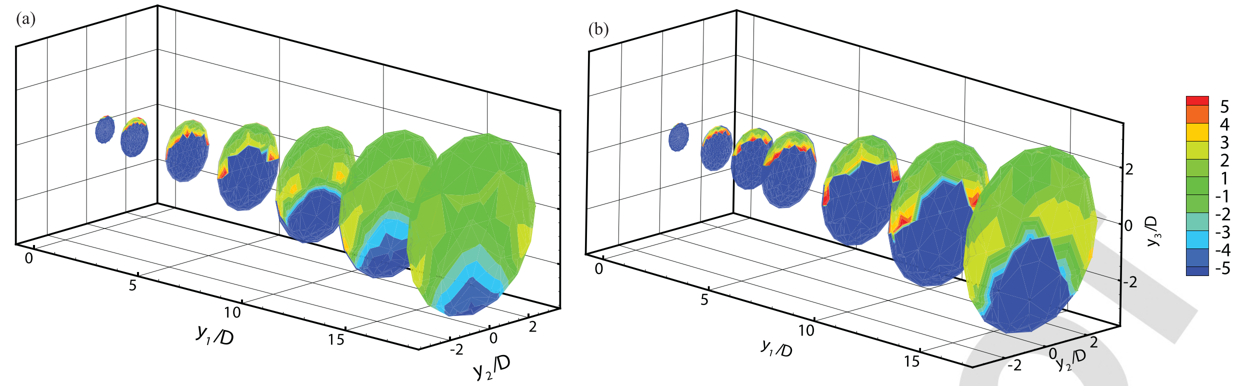

FIG. 9. (Color online) Three-dimensional visualization of flow factor for $M = 0.75$ with different temperature ratios: (a) TR = 1, (b) TR = 2.5. Far-field observer at $\theta = 50^\circ$ and $\varphi = 0^\circ$.

very small refraction effects due to the sound and flow interactions. At small polar angles, Figs. 8(a) and 8(b), however, the regions close to the nozzle, where the velocity gradient is large, is significantly affected. Increasing the temperature ratio has also been shown to increase the level of refraction effects. The flow factor results over the $y_1 - y_2$ planes at different axial locations for an observer located at $\varphi = 90^\circ$ and $\theta = 50^\circ$ are presented in Fig. 9. The results clearly show that the refraction due to the sound-flow interaction in an axisymmetric jet flow is not axisymmetric and the sources located on the opposite side of the observer suffer more refraction effects. As observed in Fig. 8, increasing the jet temperature ratio increases the region of the jet affected by refraction, Fig. 9(b).

E. Far-field noise directivity

To assess the ray-tracing based propagation model developed here, the far-field SPL results at different polar angles are presented for different Mach numbers, $M = 0.5$, 0.75, and 1.00, at TR = 1, see Fig. 10. Results are presented for observers outside the zone of silence at $\theta = 60^\circ$ and 110° from the jet axis. Results show that the far-field noise can be generally captured well for observers outside the zone of silence using the source and refraction model. The issue of propagation into the zone of silence and the limitations of the method will be discussed later.

Having shown that both the spectral behavior of the far-field noise at 90° (Fig. 5) and at different polar angles (Fig. 10), and also the Flow Factor at different jet operating conditions (Figs. 7–9), we shall now study the overall sound pressure level (OASPL) for polar angles in the range of 30°–120°, see Figs. 11 and 12. Figure 11 shows the OASPL AQ7 results for jets at $M = 0.5$ and 0.75 at different temperature ratios (TR = 1.0, 1.5, 2, and 2.5). Results for a $M = 0.5$ jet show that the critical angle in the case of TR = 1 occurs at about 46° and it moves to higher angles with temperature ratio. As expected, the model fails to predict the far-field noise within the zone of silence, but provides very good agreement at angles greater than the critical angle. The far-field noise comparisons for a $M = 0.75$ jet also show that the model developed in this work is capable of predicting the OASPL very accurately outside the zone of silence. It can also be seen from the experimental data that the far-field

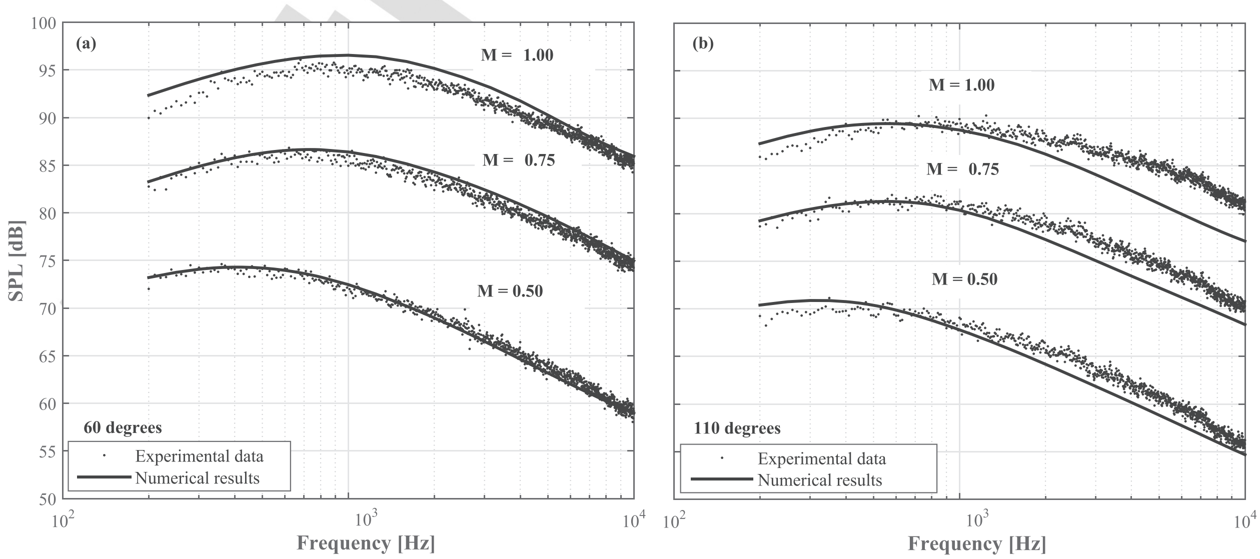

FIG. 10. Far-field SPL predictions and measurements at 60° and 110° for the isothermal jet with different M: (a) $\theta = 60^\circ$, (b) $\theta = 110^\circ$.

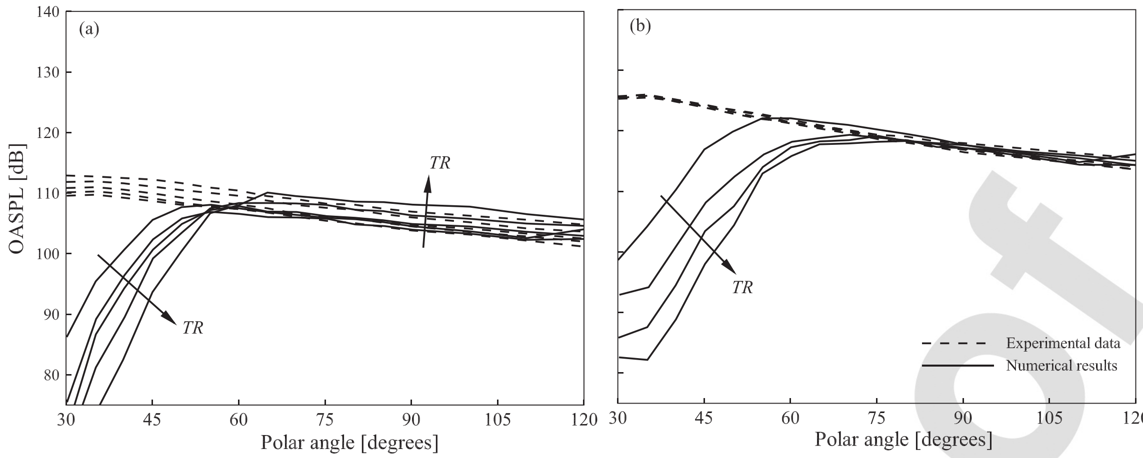

FIG. 11. OASPL prediction (solid lines) and measurements (dashed lines) for (a) $M = 0.5$ and (b) $M = 0.75$ with temperature ratio ranging from 1.0 to 2.5.

noise is more sensitive to temperature ratio at low Mach numbers ($M = 0.5$), and that the source and propagation models have managed to predict this effect well.

IV. CONCLUSIONS

In this paper an application of the LAA to model the sources of jet mixing noise coupled to a ray tracing method to compute effects of refraction is presented. The resulting method is a promising solution to quickly evaluate the noise emitted by jets from arbitrary nozzle geometries. This is particularly desired in an industrial context as it relies on the standard RANS $k - \varepsilon$ solution and makes no further assumption about the flow. Despite the need of calibration with far-field measurements, only two coefficients are needed instead of three as it is usually the case for similar methods from the literature. The coefficients are fixed for isothermal jets in the subsonic regime, however one of them needs to be changed with increasing temperature ratio; such need is understood to result from the neglect of the enthalpy source arising in AQ8 heated jets.[42–47]

Results show that the method proposed in this paper captures well the contribution of fine-scale turbulence to jet mixing noise in the subsonic regime down to a polar angle of 50°, below which the effect of a shadow zone invalidates the real ray tracing assumption. Such range of observer angles (above 50°) give valuable information if a quick estimation of the impact of non-axisymmetric geometries is sought. It thus satisfies the requirement of a design tool, presenting reasonable accuracy at relatively low computational cost while being able to consider general three-dimensional nozzle geometries.

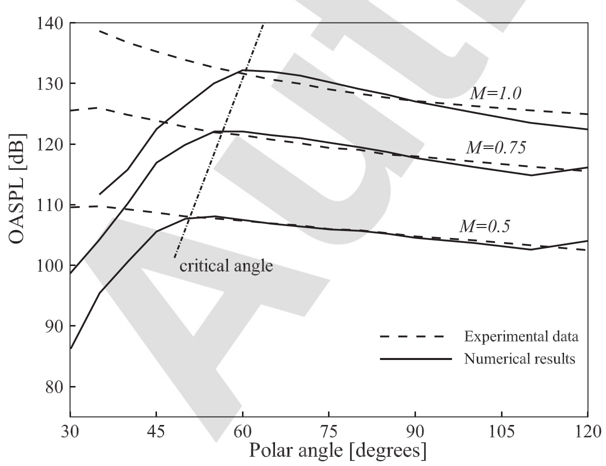

FIG. 12. OASPL prediction (solid lines) and measurements (dashed lines) at TR = 1.0 with Mach number ranging from 0.5 to 1.0. The critical angle is shown to increase linearly with M.

ACKNOWLEDGMENTS

The authors thank the financial support from CAPES, FAPESP, and EMBRAER. This research has been conducted using data from the SYMPHONY project, which is part of the UK Technology Strategy Board Contract No. TP11/HVM/6/I/AB201K.

[1]D. Papamoschou and M. Debiasi, "Directional suppression of noise from a high-speed jet," AIAA J. **39**(3), 380–387 (2001).
[2]J. Bridges and C. A. Brown, "Parametric testing of chevrons on single flow hot jets," in *Proceedings of the 10th AIAA/CEAS Aeroacoustics Conference*, AIAA Paper No. 2004–2824 (2004).
[3]D. Papamoschou, "New method for jet noise reduction in turbofan engines," AIAA J. **42**(11), 2245–2253 (2004).
[4]K. Viswanathan, M. Shur, M. Strelets, and P. R. Spalart, "Numerical prediction of noise from round and beveled nozzles," in *Proceedings of the EUROMECH Colloquium 467: Turbulent Flow and Noise Generation* (2005).
[5]ESDU International plc, "ESDU 98019 and software B9819: Computer-based estimation procedure for single-stream jet noise" (1998).
[6]J. B. Freund, "Noise sources in a low-Reynolds-number turbulent jet at Mach 0.9," J. Fluid Mech. **438**, 277–305 (2001). AQ9
[7]C. Bogey, S. Barré, D. Juvé, and C. Bailly, "Simulation of a hot coaxial jet: Direct noise prediction and flow-acoustics correlations," Phys. Fluids **21**(3), 035105 (2009).
[8]H. Xia, P. G. Tucker, and S. Eastwood, "Large-eddy simulations of chevron jet flows with noise predictions," Int. J. Heat Fluid Fl. **30**(6), 1067–1079 (2009).
[9]T. F. Balsa and P. R. Gliebe, "Aerodynamics and noise of coaxial jets," AIAA J. **15**(11), 1550–1558 (1977).
[10]T. F. Balsa, P. R. Gliebe, R. A. Kantola, R. Mani, E. J. Stringas, and J. C. F. Wang, "High velocity jet noise source location and reduction. Task 2: Theoretical developments and basic experiments," Technical Report FAA-RD-76-II, Federal Aviation Administration (1978).
[11]G. M. Lilley, "The generation and radiation of supersonic jet noise. Vol. IV—Theory of turbulent generated jet noise, noise radiation from upstream sources, and combustion noise. Part, I. I. Generation of sound in a mixing region," Technical report, Air Force Propulsion Laboratory (1972).

[12]A. Khavaran, E. A. Krejsa, and C. M. Kim, "Computation of supersonic jet mixing noise for an axisymmetric cd nozzle using k-epsilon turbulence model," in *Proceedings of the 30th Aerospace Sciences Meeting and Exhibit*, AIAA Paper No. 92-0500 (1992).

[13]A. Khavaran and E. A. Krejsa, "Role of anisotropy in turbulent mixing noise," AIAA J. **37**(2), 832–941 (1998).

[14]C. K. W. Tam and L. Auriault, "Jet mixing noise from fine-scale turbulence," AIAA J. **37**(2), 145–153 (1999).

[15]P. J. Morris and F. Farassat, "Acoustic analogy and alternative theories for jet noise prediction," AIAA J. **40**(4), 671–680 (2002).

[16]R. H. Self, "Jet noise prediction using the Lighthill acoustic analogy," J. Sound Vib. **275**(3–5), 757–768 (2004).

[17]M. Harper-Bourne, "Jet near–field noise prediction," in *Proceedings of the 5th AIAA/CEAS Aeroacoustics Conference and Exhibit*, AIAA Paper No. 99-27825 (1999).

[18]R. H. Self and M. Azarpeyvand, "Utilization of turbulent energy transfer rate time-scale in aeroacoustics with application to heated jets," Int. J. Aeroacoust. **7**(2), 83–102 (2008).

[19]R. H. Self and M. Azarpeyvand, "Jet noise prediction using different turbulent scales," Acoust. Phys. **55**(3), 433–440 (2009).

[20]M. Azarpeyvand and R. H. Self, "Improved jet noise modeling using a new time-scale," J. Acoust. Soc. Am. **126**(3), 1015–1025 (2009).

[21]S. M. Candel, "Numerical solution of conservation equations arising in linear wave theory: Application to aeroacoustics," J. Fluid Mech. **83**(3), 465–493 (1977).

[22]J. B. Freund and T. G. Fleischman, "Ray traces through unsteady jet turbulence," Int. J. Aeroacoust. **1**(1), 83–96 (2002).

[23]P. R. Spalart, M. L. Shur, and M. Kh. Strelets, "Identification of sound sources in large-eddy simulations of jets," in *Proceedings of the 13th AIAA/CEAS Aeroacoustics Conference*, AIAA Paper No. 2007-3616 (2007).

[24]X. Xu, J. He, X. Li, and F. Q. Hu, "3-D jet noise prediction for separate flow nozzles with pylon interaction," in *Proceedings of the 53rd AIAA Aerospace Sciences Meeting*, AIAA Paper No. AIAA 2015-0512 (2015).

[25]M. J. Lighthill, "On sound generated aerodynamically. I. General theory," Proc. Roy. Soc. A **211**, 564–587 (1952).

[26]H. S. Ribner, "Quadrupole correlations governing the pattern of jet noise," J. Fluid Mech. **38**(1), 1–24 (1969).

[27]G. K. Batchelor, *The Theory of Homogeneous Turbulence* (Cambridge University Press, Cambridge, 1953).

[28]C. Bailly, W. Béchara, and P. Lafon, "Jet noise prediction using a k-epsilon turbulence model," in *Proceedings of the 15th AIAA Aeroacoustics Conference*, AIAA Paper No. 93-4412 (1993).

[29]P. A. Lush, "Measurements of subsonic jet noise and comparison with theory," J. Fluid Mech. **46**(3), 477–500 (1971).

[30]A. D. Pierce, *Acoustics: An Introduction to its Physical Principles and Applications* (McGraw-Hill, New York, 1981).

[31]D. Blokhintzev, "The propagation of sound in an inhomogeneous and moving medium I," J. Acoust. Soc. Am. **18**(2), 322–328 (1946).

[32]H. Kenner, *Geodesic Math and How to Use It* (University of California Press, Oakland, CA, 1976).

[33]M. J. Wenninger, *Spherical Models* (Cambridge University Press, Cambridge, 1979).

[34]S. Y. Seidel, "Site-specific propagation prediction for wireless in-building personal communication system design," IEEE Trans. Vehicular Technol. **43**(4), 879–891 (1994).

[35]ANSYS Inc., Canonsburg, PA, Product Documentation Release 14.0 (2010).

[36]C. K. W. Tam and A. Ganesan, "Modified k-epsilon turbulence model for calculating hot jet mean flows and noise," AIAA J. **42**(1), 26–34 (2004).

[37]P. O. Witze, "Centerline velocity decay of compressible free jets," AIAA J. **12**(4), 417–418 (1974).

[38]P. J. Morris and S. Boluriaan, "The prediction of jet noise from CFD data," in *Proceedings of the 10th AIAA/CEAS Aeroacoustics Conference*, AIAA Paper No. 2004-2977 (2004).

[39]M. Omais, S. Redonnet, B. Caruelle, and E. Manoha, "Jet noise prediction using RANS CFD input," in *Proceedings of the 5th AIAA/CEAS Aeroacoustics Conference*, AIAA Paper No. 2008-2938 (2008).

[40]S. A. Karabasov, M. Z. Afsar, T. P. Hynes, A. P. Dowling, W. A. McMullan, C. D. Pokora, G. J. Page, and J. J. McGuirk, "Jet noise: Acoustic analogy informed by Large Eddy Simulation," AIAA J. **48**(7), 1312–1325 (2010).

[41]N. K. Depuru Mohan, A. P. Dowling, S. A. Karabasov, H. Xia, O. Graham, T. P. Hynes, and P. G. Tucker, "Acoustic sources and far-field noise of chevron and round jets," AIAA J. **53**(9), 2421–2436 (2015).

[42]M. E. Goldstein, *Aeroacoustics* (McGraw-Hill, New York, 1976).

[43]R. H. Self, "A RANS CFD coupled model for predicting coaxial jet noise," ISVR Internal Technical report No. 304, Institute of Sound and Vibration Research, Southampton, U. K. (2005).

[44]C. R. S. Ilário, "Development of a novel RANS-based method for the computational aeroacoustics of high speed jets," Ph.D. thesis, Universidade de São Paulo, São Paulo, 2011.

[45]R. C. Engel, C. R. S. Ilário, and C. J. Deschamps, "Application of RANS-based method to predict acoustic noise of chevron nozzles," Appl. Acoust. **79**, 153–163 (2014).

[46]G. M. Lilley, "The radiated noise from isotropic turbulence with applications to the theory of jet noise," J. Sound Vib. **190**(3), 463–476 (1996).

[47]J. T. Stone, R. H. Self, and C. J. Howls, "A complex ray-tracing tool for high-frequency mean field flow-interaction effects in jets," in *Proceedings of the 20th AIAA/CEAS Aeroacoustics Conference*, AIAA Paper No. 2014-2757 (2014).